PHYSICAL REVIEW B VOLUME 34, NUMBER 10 15 NOVEMBER 1986

rf-sputtered B-doped *a*-Si:H and *a*-Si-B-H alloys

D. Jousse, E. Bustarret, and A. Deneuville
Laboratoire d'Etudes des Propriétés Electroniques des Solides du Centre National de la Recherche Scientifique, Université Scientifique, Technologique et Médicale de Grenoble, Boîte Postale No. 166, 38042 Grenoble Cédex, France

J. P. Stoquert
Laboratoire de Phase, Centre de Recherche Nucléaire, Boîte Postale No. 20, 67037 Strasbourg Cédex, France
(Received 3 July 1986)

Amorphous silicon films have been sputtered in an Ar-H_2 mixture over a wide range of B_2H_6 concentrations $Y_g(=[B_2H_6]/([Ar]+[H_2]))$. The chemical composition of the films has been determined. H bonding was analyzed by ir spectroscopy. Besides electrical and optical properties, disorder and defects were characterized by photothermal deflection spectroscopy (PDS) as well as equilibrium (ESR) and light-induced electron-spin resonance (LESR). The incorporation of boron is linear and three distinct regimes are found for the relationship between doping and defects. At low doping ratios, the hydrogen content increases and H is preferably incorporated in isolated sites. The progressive elimination of clustered H (or microvoids) can be correlated with a decrease of the gap defect density N_R and a widening of the valence-band tail followed by PDS. An N_R value of 5×10^{16} cm^{-3} has been achieved for a B content N_B of 5×10^{18} cm^{-3} which is a progress compared to equivalent glow-discharge *a*-Si:H. For $Y_g\geq10^{-4}$, the valence-band tail broadens and the defect density increases linearly according to $N_R=N_B/100$ in contrast with the square-root dependence found in glow-discharge films. The difference is explained by the important role of the ionic bombardment as compared to the surface reactions in the sputtering technique. LESR results show that the doping-induced defects are mainly Si dangling bonds. The narrowing of the optical gap for $Y_g=10^{-3}$ is primarily ascribed to Si—B bonds involving threefold coordinated B atoms as the loss of hydrogen is shown to be a secondary effect. Nonconducting alloys with nearly equal quantities of Si, B, and H are obtained by $Y_g=10^{-2}$. They contain a high fraction of polyhydride units and bridging B—H—B or B $\cdots$ H—Si bonds leading to low-density materials.

I. INTRODUCTION

The capability of doping hydrogenated amorphous silicon (*a*-Si:H) prepared either by the glow-discharge[1] or sputtering[2] techniques has played an historical role in the spreading of research in this field. But, it is striking that ten years later, nearly all the doping studies that can be found in the literature concern the glow-discharge (GD) material[3–6] except that of Anderson and Paul[7] on P doping of rf sputtered (SP) material. Obviously the rapid success of the GD technique in amorphous silicon technology has eclipsed the parallel but less spectacular improvements in photovoltaic performances of SP *a*-Si:H solar cells.[8–10] In a recent study on undoped SP *a*-Si:H, the authors[11] have concluded the existence of other defects than dangling bonds from the comparison of electron-spin resonance (ESR) and photothermal deflection spectroscopy (PDS) results. The correlation between the density of these extra defects and the fraction of hydrogen in clustered SiH units[11,12] suggests a stronger tendency to form microvoids (or hydrogenated multivacancies) which could explain the common observation of inferior electronic quality of the SP material.

The present paper reports on the first detailed investigation of the properties of B-doped *a*-Si:H and *a*-Si-B-H alloys prepared by the rf sputtering technique with an emphasis on the correlation between defect densities and physicochemical properties. The elemental composition of the films was checked by B secondary-ion mass spectroscopy (SIMS) and H nuclear measurements. Infrared absorption was used for the analysis of the different H and B bondings. Fermi-level shifts and changes in the optical gap were followed by dark conductivity and visible transmission measurements, respectively. Disorder and gap defects characterization was made by PDS and ESR measurements. Such a systematic and extensive approach through various complementary techniques is actually necessary to understand various doping effects which are often mixed together. In particular, the studies on B-doped GD *a*-Si:H (Refs. 4–6 and 13–19) have left a certain number of unsolved questions that will be addressed here: How are the changes of the optical gap related to the hydrogen contents, the local order, and the Si-B alloying effects? Are there other defects than dangling bonds and what are their dependencies on the dopant concentration? Is the dangling-bond energy modified by the incorporation of dopants?

At very high doping levels, a hydrogen-rich silicon-boron alloy is obtained which presents properties very different from B-doped *a*-Si:H. Their properties will be dis-

 ©1986 The American Physical Society

cussed and compared to those on similar alloys obtained by the glow-discharge technique.[4]

The preparatory details are given in Sec. II. Three sections deal with the results analysis which are devoted to the physicochemical description of the materials (Sec. III), the optical and electrical properties (Sec. IV), and the disorder and defect characterization by PDS and ESR (Sec. V). A general discussion follows in Sec. VI. The main results and conclusions are summarized in Sec. VII.

II. EXPERIMENTAL DETAILS

The 1 μm thick samples have been prepareed by rf sputtering of a polycrystalline silicon target in a reactive mixture of 80 vol% Ar, 20 vol% H_2, and fractions of B_2H_6. In the following, the gas phase concentrations are defined from partial pressures through $Y_g=[B_2H_6]/([Ar]+[H_2])$ and were increased from 10^{-6} to 10^{-2} to prevent residual dopant contamination. Previous studies in this laboratory on the undoped material[20,21,11] have shown that a low deposition rate and substrate temperatures T_s between 150 and 250 °C lead to a material which appears free of microstructure under the electron microscope and presents a minimum overall density of defects: dangling bonds and clustered H related defects. A deposition rate of 30 Å/min was obtained for a dc target voltage of 600 V. The deposition rate was not affected by the inclusion of B_2H_6 up to $Y_g=10^{-3}$ but decreased down to 15 Å/min for $Y_g=10^{-2}$. Two series of samples were deposited, one at 190 and the other at 250 °C. Other constant parameters were the base pressure (2×10^{-6} Torr), the total pressure during deposition (8 mTorr), the gas flow (1.2 1/h), and the substrate to target distance (5 cm). Double-polished highly resistive and n-type c-Si substrates were used for ir spectroscopy or nuclear measurements and SIMS profiling, respectively. Fused silica and common glasses were used for optical or ESR and electrical measurements, respectively.

Most of the experimental techniques that have been used for the present study are already well known for a-Si:H. References and additional details will be given when necessary along with the analysis of the results.

III. PHYSICOCHEMICAL CHARACTERIZATION

A. B and H contents

Boron concentrations in the films were measured by SIMS with a primary beam of $^{32}O_2^+$ ions and a SMI 300 CAMECA analyzer. The technique is very accurate in the intermediate doping range. It gives only a rough estimation for low-B contents and appeared unsuitable for the a-Si-B-H alloys. In this last case, the B sputtering rate was not known and nonuniform sputtering has resulted in large craters. For B-doped a-Si:H, the depth profiles indicate that the film composition is uniform throughout the thickness except at the lowest B contents where the B concentration at the surface may exceed the bulk value by a factor of 5. The results are given in Fig. 1 with the magnitude of error. The B incorporation is linear versus nominal doping and independent of temperature in the investigated range. The incorporation efficiency is relatively high: 1 vppm B_2H_6 in the reactive gas leads to a B/Si ratio of 20 at. ppm. The extrapolation of the curve to $Y_g=10^{-2}$ would give a B/Si ratio of 1 (dotted line).

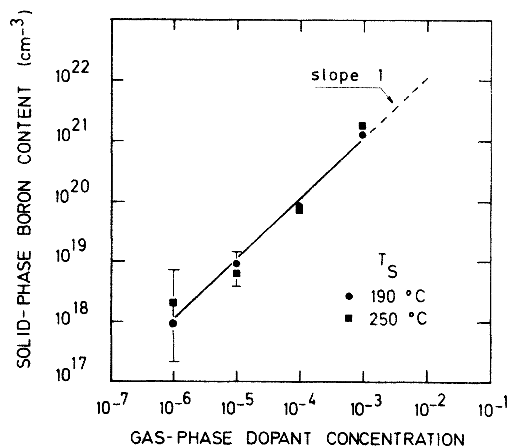

FIG. 1. Boron concentrations in the film measured by SIMS versus nominal doping.

We have also checked the dopant concentration in nominally "undoped" samples deposited after some runs at $Y_g=10^{-2}$. We have found $N_B\sim2\times10^{19}$ cm^{-3}, a B content that would correspond to $Y_g=3\times10^{-5}$ which shows the importance of our procedure of depositing the samples only in increasing Y_g. The remanence of the dopant was attributed to the reactivity of the grain boundaries of the polycrystalline Si target.

The resonant nuclear reaction with ^{15}N is the most reliable tool for profiling the H concentration in the film thickness. It also gives an absolute value of the total H content irrespective of the H sites. Figure 2 shows the H profiles for samples deposited at 190 °C. The H percentages on the right-hand scale have been calculated by assuming a constant total atomic concentration of 5×10^{22} cm^{-3}. A good uniformity is obtained for doping levels above 10^{-5} while a peak in H concentration for the first 1000 Å is well defined at $Y_g=10^{-6}$ and also present in the undoped sample. Similar results are obtained in the series of samples deposited at 250 °C. The accumulation

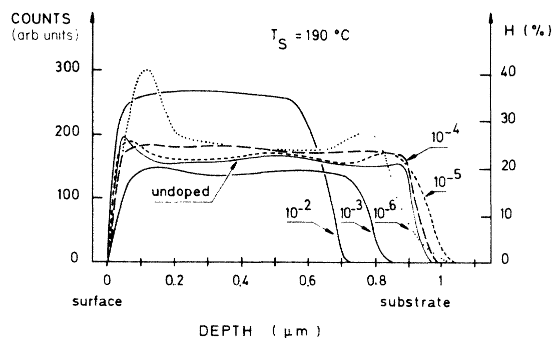

FIG. 2. Hydrogen profiles as a function of film depth from nuclear reaction method for SP a-Si:H deposited at $T_s=190$ °C and boron doping levels Y_g between 0 and 10^{-2}.

of H near the surfaces seems to be a specific property of the most intrinsic samples. We have no clear explanation for it at this moment. For $Y_g > 10^{-5}$ boron doping favors a very homogeneous distribution of H throughout the film thickness.

More striking is the marked increase of the mean hydrogen content between the undoped and 10^{-6} doped samples as shown in Fig. 3. This effect was already mentioned in our preliminary studies on doping of SP a-Si:H (Ref. 22) and since has also been observed in B-doped GD a-Si:H.[14,15,18] On one hand, the H atoms brought in the plasma by the B_2H_6 molecules at 1-vppm concentration cannot account for the observed enhancement without a catalytic effect of B_2H_6 on the inclusion of H in the silicon network at the growing surface. On the other hand, H incorporation decreases when the B concentration in the film or the substrate temperature increases which suggests that B atoms, like high T_s, enhance the desorption of the superficial hydrogen from the film. Another possibility to explain the lowest H content at $Y_g = 10^{-3}$ would be a preferential attachment of H to Si rather than B as will be discussed in Sec. III B 1. The situation is different in a-Si-B-H alloys. They contain high-H concentrations with other kinds of bonding configurations as will be seen from the ir spectra. In this latter case, hydrogen is more loosely bonded and, according to Fig. 3, its concentration depends strongly on T_s.

B. ir absorption

1. B-doped a-Si:H

ir absorption was calculated from the ir transmission spectrum recorded with a double beam Perkin-Elmer spectrophotometer. The absorption spectra of B-doped films up to $Y_g = 10^{-3}$ are very similar to those of undoped films. Typical examples are given in Fig. 4 which shows the three usual vibrational modes. According to the classical interpretation,[23–25] the line at 630 cm^{-1} is due to the wagging mode of vibration for all the Si—H bonds while the absorption at 890 cm^{-1} is due to the bending mode of SiH_2 units. The satellite line at 845 cm^{-1} indicates the presence of some $(SiH_2)_n$ units. The

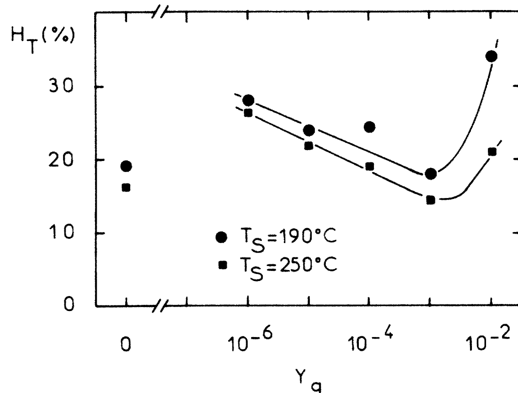

FIG. 3. Dependence of the mean total hydrogen content in the films upon boron doping.

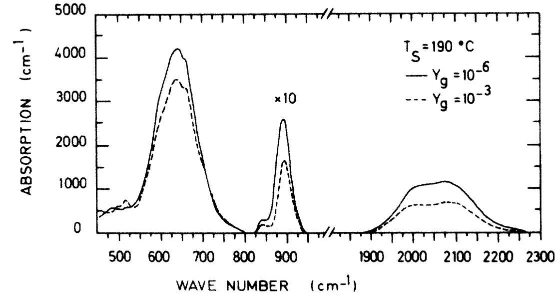

FIG. 4. Infrared absorption spectra of SP a-Si:H doped at $Y_g = 10^{-6}$ and 10^{-3}.

deconvolution of the stretching doublet around 2000 cm^{-1} in two Gaussian peaks yields one line at 2000 cm^{-1} due to the stretching mode of SiH units[23] and the other one at 2095 cm^{-1} that may originate either from SiH_2 units or clustered Si—H units.[26,27] The presence of a bending mode in our samples clearly indicates that we have SiH_2 groups. The existence of clustered Si—H units is evidenced only by the fact that the intensity of the 2095-cm^{-1} mode does not scale with that of the 890-cm^{-1} mode as shown below.

A detailed analysis of the spectra revealed variations in the relative intensities of the different modes with doping. The percentages of H in the different bondings can be estimated if the respective oscillator strengths are known. The different concentrations H_W, $H_{2000\,cm^{-1}}$ and $H_{2095\,cm^{-1}}$ are related to the respective integrated normalized absorptions at 630, 2000, and 2095 cm^{-1} by

$$H_{W,\,2000\,cm^{-1},\,2095\,cm^{-1}} = K_{W,2000\,cm^{-1},\,2095\,cm^{-1}} \times \int \frac{\alpha(\omega)}{\omega} d\omega \,, \quad (1)$$

with the following constants: $K_W = 0.032$, $K_{2000\,cm^{-1}} = 0.282$, and $K_{2095\,cm^{-1}} = 0.187$. The constants were determined from the literature and calibration with nuclear reactions.[28] We also define $H_S = H_{2000\,cm^{-1}} + H_{2095\,cm^{-1}}$ which has been sometimes used as a measure of the total hydrogen content. The oscillator strengths are sensitive to the bonding environment and thus possibly to doping. The changes can be detected when the H content is independently known from the nuclear reaction. The results are summarized in Fig. 5 for the set of samples deposited at $T_S = 190\,°C$. Also given are the variations of the integrated area of the bending mode $I_{890\,cm^{-1}}$ with doping. We verify, at least for low-and intermediate-B contents, that H_W is a better estimate of the total H content than H_S in agreement with Shanks *et al.*[26] and our previous results on undoped SP films.[21] The proportionality constants that we used for the determination of H_S lead to a systematic underestimation by a factor of 1.2 because they are appropriate only for SP a-Si:H deposited at T_s below 150 °C.[21] If we consider now the different types of H bondings, we note that both $H_{2000\,cm^{-1}}$ and $I_{890\,cm^{-1}}$ go through a maximum between $Y_g = 10^{-6}$ and 10^{-5}. If the interpretation of $H_{2095\,cm^{-1}}$ as the sum of two contributions (SiH_2+ clustered SiH units) is correct, then,

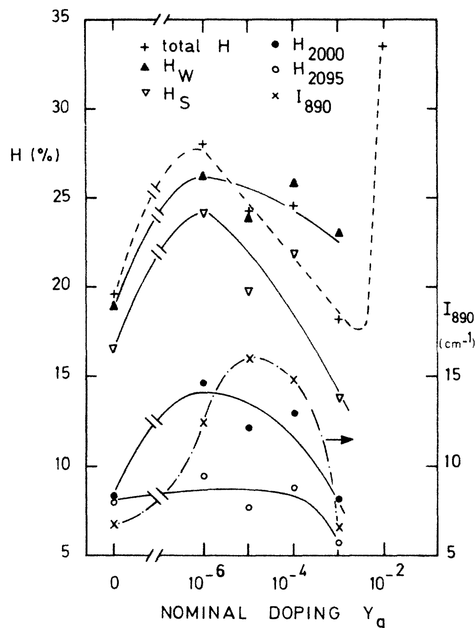

FIG. 5. Hydrogen concentrations on the various sites from ir spectroscopy in B-doped SP a-Si:H at the different doping levels ($T_s = 190$ °C).

the results show that the concentration of H in the clustered form goes through a minimum around 10^{-5}. The excess hydrogen incorporated into the films at moderate doping is preferably bonded as SiH or SiH_2. The decrease in the concentration of clustered H corresponds to a more homogeneous material with a reduced density of hydrogenated Si vacancies or microvoids and less fluctuations in the local H density. Finally, we have not observed any shift in the position of the absorption lines even at $Y_g = 10^{-3}$, i.e., for a [B]/[Si] ratio of 1/50. This confirms that there are no charge effects due to the vicinity of B atoms,[29] at least up to that concentration. So, the use of the same oscillator strength to compare doped samples deposited at the same temperature was a reasonable approximation. The marked decrease in $I_{890\,cm^{-1}}$ and $H_{2000\,cm^{-1}}$ as compared to $H_{2095\,cm^{-1}}$ for $Y_g = 10^{-3}$ would mean that inhomogeneity increases again in heavily doped samples.

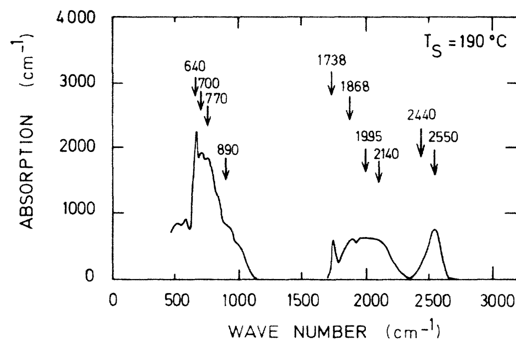

FIG. 6. Infrared absorption spectrum of an hydrogenated silicon-boron alloy deposited by sputtering at $Y_g = 10^{-2}$.

2. *a-Si-B-H alloys*

The absorption spectrum for a sample doped at $Y_g = 10^{-2}$ shown in Fig. 6 is totally different from the previous ones. It looks similar to those reported for a-Si-B-H alloys.[4,30] However, we can get additional information because in our case a fine structure is clearly revealed under the three main broadbands around 800, 2000, and 2500 cm^{-1}. The frequencies indicated in the figure are the result of a best-fit decomposition of the bands in Gaussian peaks. Most of the lines can be identified from ir studies on gas, liquid, and solid B_2H_6,[31,32] evaporated (EV) a-B:H (Refs. 33 and 34) or B-doped GD a-Si:H (Ref. 30) and GD a-Si-B-H alloys.[4] The attributions of the various lines of our SP a-Si-B-H alloys are given in Table I with the corresponding references.

The sample of Fig. 6 has approximately the composition a-$Si_{0.33}B_{0.33}H_{0.34}$ from Sec. III A. The differences between our spectrum (Fig. 6) and those of Refs. 4 and 30 may be attributed not only to the different deposition techniques but also to differences in sample compositions. In the same way, the broadband around 1900 cm^{-1} has been found in the B-rich a-Si-B-H alloys[4] and not in the highly B-doped a-Si:H with low-H content.[30] The fact that our sample contains equal quantities of the three elements explains the great variety of lines that we observe.

We justify now some features of our decomposition. The band around 2500 cm^{-1} corresponding to B—H stretching modes is clearly asymmetric and has been

TABLE I. Vibrational modes for sputtered a-Si-B-H alloys.

Absorption line (cm^{-1})	Attribution	Also observed	Reference
2550	BH_2, BH_3 stretching	at 2560 in EV a-B:H, GD a-Si-B-H	33,34,4
2440	BH stretching	at 2475 in B-doped GD a-Si:H	30
2095, 2140	SiH_2, SiH_3 stretching	in SP and GD a-Si:H	24,25
1995	SiH stretching	in SP and GD a-Si:H	23
	or B—H—B stretching	at 1984 in B_2H_6	32
1868	B · · · H—Si stretching	in H compensated B in c-Si	35,36
1738	unidentified		
890	SiH_2, SiH_3 bending	in SP and GD a-Si:H	24,25
770	BB lattice vibrations	at 776 and 796 in α-B	37
700	SiB stretching	in B-doped GD a-Si:H	30
640	SiH wagging	in SP and GD a-Si:H	24,25

decomposed in a line at 2440 cm^{-1} that we attribute to BH units[30] and another line at 2550 cm^{-1} that is ascribed to BH_2 or BH_3 units. The last attribution agrees with the occurrence of the stretching modes at 2609 and 2520 cm^{-1} in B_2H_6 and 2560 cm^{-1} in BH_3.[32] The shift of the central position of the band from 2475 cm^{-1} in B-doped GD *a*-Si:H (Ref. 30) to 2560 cm^{-1} in GD *a*-Si-B-H (Ref. 4) reflects a change from mainly monohydride units to polyhydride units when the [H]/[Si] and [B]/[Si] ratios increase at the transition between the doping and the alloying regime.

A broadband around 1900 cm^{-1} was attributed by Tsai[4] to bridging B—H—B bonds with a large distribution of bond strengths. In fact, our four Gaussian fit procedure for the 1700–2300 cm^{-1} range with all free parameters converged with a good accuracy towards line positions at 1738, 1868, 1995, and 2140 cm^{-1}. The two last lines may be attributed to other configurations, namely, SiH and SiH_3 units, respectively, although we may have missed this way other components of weaker intensity like SiH_2 at 2095 cm^{-1}. The absorption bands due to bridging B—H—B bonds occur at 1900 and 1984 cm^{-1} in B_2H_6 (Ref. 32) and the latter cannot be distinguished from the SiH band at 1995 cm^{-1}.

The line at 1868 cm^{-1} well resolved in our spectrum has never been mentioned in previous studies on alloys. But recent works on the compensation of B acceptors in *c*-Si by Pankove *et al.*[35] and Johnson[36] give exactly the same frequency for the stretching mode of a Si—H bond at the site of a substitutional boron atom. Some delocalization of the bonding electrons probably occurs giving this kind of weakly bridging bond that we call here B··· H —Si. We believe that such a configuration is highly probable in *a*-Si-B-H alloys.

Finally, let us comment on the decomposition of the band around 700 cm^{-1}. The fine structure reveals at least four components: a very narrow line at 640 cm^{-1} due to Si—H wagging vibrations, a line at 890 cm^{-1} which corresponds to the bending vibrations of SiH_2 or SiH_3 units, and two other components at 700 and 770 cm^{-1}. The line at 700 cm^{-1} is related to Si—B stretching modes according to Shen and Cardona.[30] We attribute the neighboring line at 770 cm^{-1} to B—B bonds. In fact, the most intense lattice vibrations in α-B have been found at 776 and 796 cm^{-1} from Raman spectroscopy.[37] These bonds become ir active because of the asymmetry resulting from different back bonds.

The analysis brings to the conclusion that SP *a*-Si-B-H alloys have a good cross linking of the B and Si constituents. However, they are predominantly rich in polyhydride units especially SiH_2, SiH_3, or BH_2, BH_3 which give a poor connectivity of the network that is partly ensured by bridging B··· H—Si or B—H—B bonds. The very different and somewhat inhomogeneous structure of *a*-Si-B-H alloys compared to B-doped *a*-Si:H are probably also related to the sputtering conditions. The Ar-H_2 mixture has a fixed composition and two plasma mechanisms may account for the results at 1% B_2H_6 dilution: a first effect equivalent to an increase of the hydrogen partial pressure which is known to favor the formation of a tissue-type material[38] and then, gas phase reactions due to the high diborane partial pressure.

Our last remark deals with the discontinuity between the ir spectra of samples deposited at $Y_g = 10^{-3}$ (Fig. 4) and 10^{-2} (Fig. 6). The composition of the former is a-$Si_{0.79}B_{0.03}H_{0.18}$. If the H incorporation process were similar for both materials, a weak line should be present at ~ 2500 cm^{-1} with an intensity tenfold reduced as compared to the signal of Fig. 6. The absence of any trace of B—H bonds at this B concentration, in contrast with the results for GD B-doped *a*-Si:H,[30] suggests that in sputtered films H is preferably attached to Si in the doping regime. This is no longer true in the alloy regime where the intensities of the SiH and BH lines are comparable. As a confirmation, we have observed parallel reductions in the intensities when T_s increases from 190 to 250 °C.

IV. OPTICAL AND ELECTRICAL PROPERTIES

A. Optical-absorption edge and refractive index

At all doping levels, the optical-absorption coefficient α derived from optical transmission spectrum followed the Tauc relation for photon energies $h\nu$ higher than 2 eV,

$$(\alpha h\nu)^{1/2} = B_0(h\nu - E_G) . \quad (2)$$

The variations with doping of the optical gap E_G and absorption-edge parameter B_0 are shown in Fig. 7 for the two series of samples. Both quantities present a maximum at $Y_g = 10^{-5}$ for samples deposited at $T_s = 250$ °C and 10^{-4} for $T_s = 190$ °C. The other salient feature is the rapid narrowing of the optical gap from 1.75 to 1.5 eV when doping is increased from 10^{-4} to 10^{-3}. It is a general property which is well known for GD *a*-Si:H (Refs. 18 and 19) and two different models have been proposed: a Si-B alloying effect[4] and a reduction of the H content in the films.[18,19] The comparison between the variations of H content (Fig. 3) and E_G [Fig. 7(a)] with Y_g shows clear-

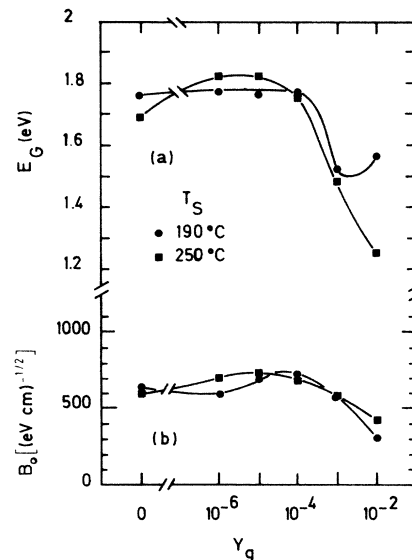

FIG. 7. Variations of the optical gap E_G (a) and absorption-edge parameter B_0 (b) with boron doping.

ly that there is no quantitative correlation. In particular, higher E_G values have been obtained in materials deposited at 250 °C which contain less hydrogen. As will be discussed in Sec. VI, structural and chemical disorder considerations are sufficient to explain the variations of E_G in all the doping range. The narrowing of E_G by Si-B alloying is confirmed by the continuity of the decrease in E_G for samples deposited at 250 °C from doping (10^{-4}) to alloy regime (10^{-2}). The H content remains around 20% and the main change is the [B]/[Si] ratio which increases from 0.2 to 45%. In contrast with doped samples, the optical gap of a-Si-B-H alloys appears to be very dependent on the H content if we compare the results for $T_s = 190$ and 250 °C. This is in good agreement with results on a-B:H showing variations between 1.0 eV for a-B (Ref. 39) and 2.19 eV for a-B:H (Ref. 40) according to the H content.

The refractive index at low energies n_s was calculated from the transparent region of the transmission spectrum. The data of Fig. 8(a) show that it depends also on doping. n_s increases from 2.95 up to 3.1 between undoped and 10^{-3} doped materials. An increase in n_s is indeed expected if a higher density material is achieved by the elimination of microvoids as indicated by the ir hydrogen sites analysis. In the absence of direct density measurements, we shall use the approach proposed by Freeman and Paul.[24] n_s is related to the Penn gap by the relation

$$n_s^2 - 1 = 4\pi \mathcal{N} e^2 \hbar^2 / m E_P^2 \, , \tag{3}$$

where $\mathcal{N}$ is the density of valence-band states per cm^3 and other quantities are classical constants. Assuming parallel variations for E_P and E_G with doping, we can use the product $(n_s^2 - 1)E_G^2$ to follow qualitatively the variations in density with doping. The results plotted in Fig. 8(b) show clearly that the density increases up to $Y_g = 10^{-4}$ for $T_s = 190$ °C and 10^{-5} for $T_s = 250$ °C. The rapid decrease in the alloy regime agrees with the poor connectivity and the multiple hydrogen bondings seen in the ir analysis. Indeed, the n_s values for our SP a-Si-B-H alloys are much lower than the 3.35 value for evaporated a-B.[39]

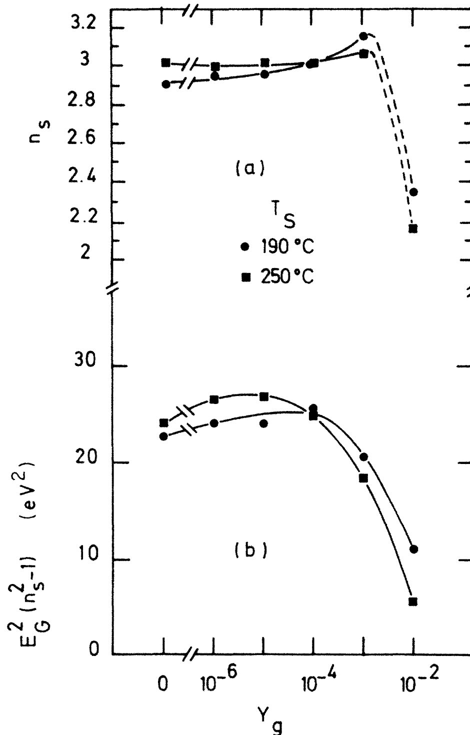

FIG. 8. (a) Variations of the low-energy refractive index n_s versus dopant concentration; (b) qualitative variations of the film density in the form $(n_s^2 - 1)\,E_G^2$.

B. Conductivity

The conductivity was measured in the gap cell configuration with a Keithley 616 electrometer. Two gold-antimony electrodes of 1.2 cm length were evaporated 1.4 mm apart on the top of the film. Annealing of the samples during one hour at 190 °C in the dark was done previously to the measurements to remove surface adsorbates or light-induced effects.

The variations of the dark conductivity at 300 K, σ_{RT}, are given in Fig. 9 for the two series of samples and the $\log_{10} \sigma$ versus $1/T$ curves for samples deposited at 190 °C are given in Fig. 10. The lowest σ_{RT} values of $\sim 10^{-13}$ $(\Omega\,\mathrm{cm})^{-1}$ on lightly doped samples have been derived from the extrapolation of the conductivity curves. Except for $Y_g = 10^{-2}$ the conductivity curves display an activated behavior for $T > 300$ K in lightly doped samples and $T > 400$ K at high doping. The corresponding activation energies E_a and pre-exponential factors σ_0 are shown in Fig. 11 as a function of nominal doping. These are assumed to represent extended states transport. We have also tried to get E_a by the procedure proposed by Beyer and Overhof[6] from $E_a = 0.0258 \ln(100/\sigma_{RT})$ and obtained identical values within 50 meV. The thermoelectric power at 300 K has been measured on samples deposited at 250 °C and doped with $Y_g = 10^{-6}$ and 10^{-3}. The values of $+1.23$ and $+0.63$ mV K^{-1}, respectively, indicate that the samples are p type even at the lowest nominal doping. A well-known limitation of conductivity coplanar measurements, i.e., interface or surface accumulation layers[41] can be disregarded here as we have measured

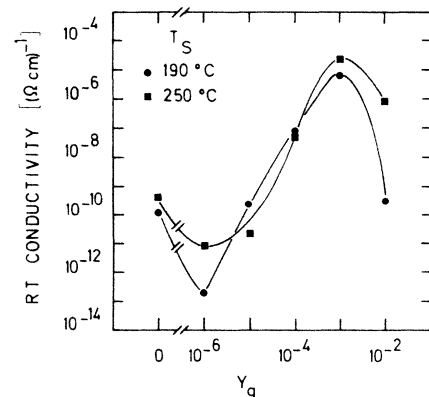

FIG. 9. Room-temperature conductivity as a function of dopant concentration for B-doped SP a-Si:H.

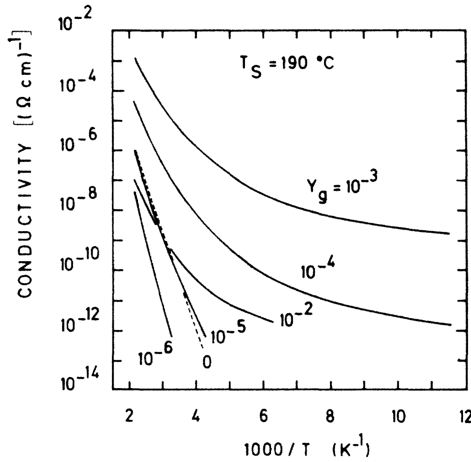

FIG. 10. Plots of $\log_{10}\sigma$ versus $1/T$ for undoped, B doped at different levels and B alloyed SP a-Si:H.

exactly $E_a = E_G/2$ in the most intrinsic samples ($Y_g = 10^{-6}$). There remains a possibility of depletion layers without great consequence because the space-charge zones are much shorter than the sample thickness according to our densities of gap defects (Sec. V). From these arguments, the variations of E_a in Fig. 11(a) reflect the variations of $E_F - E_V$ with doping.

As it is the first detailed study on gas phase B doping of RF sputtered a-Si:H it is interesting to compare briefly our conductivity results to those achieved by other deposition techniques. The highest σ_{RT} values of 2×10^{-5} $(\Omega\,\text{cm})^{-1}$ and lowest $E_a = 0.35$ eV for $Y_g = 10^{-3}$ and $T_s = 250\,°\text{C}$ compare fairly well with the first published results on B doping of GD a-Si:H by Spear and LeComber.[3] Conductivities have been increased since, after a careful optimization of deposition conditions for

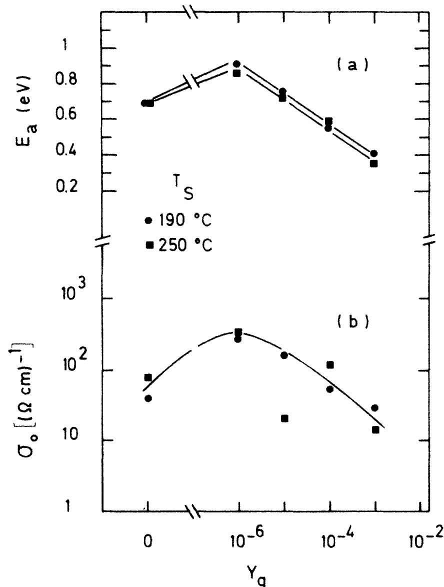

FIG. 11. Conductivity activation energy (a) and pre-exponential factor (b) as a function of dopant concentration.

GD material. We should like to mention here a result by Moustakas[42] which gives a maximum σ_{RT} of 10^{-4} $(\Omega\,\text{cm})^{-1}$ and minimum E_a of 0.27 eV for a SP a-Si:H which was also doped by the gas phase although the exact conditions were not given. Sputtered films doped in a different way have also exhibited similar conductivities: $\sigma_{RT} = 3\times10^{-6}$ $(\Omega\,\text{cm})^{-1}$ and $E_a = 0.36$ eV by a cosputtering technique,[43] $\sigma_{RT} = 2\times10^{-5}$ $(\Omega\,\text{cm})^{-1}$ and $E_a = 0.32$ eV by sputtering of a Si target doped with 10^{19} B/cm^3.[44] However, the solid-phase dopant concentrations were not given and doping efficiencies by the solid or the gas phase cannot be compared directly. In view of the σ_{RT} curves of Fig. 9, a higher doping efficiency is obtained for films deposited at higher T_s. The boron incorporation was shown to be temperature independent (Fig. 1) but more B atoms enter in substitutional sites as the higher possibility of bonding rearrangements compensates better the defects during growth.

The results of Fig. 11(b) show that σ_0 follows qualitatively E_a. The σ_0 versus E_a variations are plotted in Fig. 12 and compared to other results. The Meyer-Neldel rule applies in our sputtered B-doped samples. A least-squares fit to our data yields $\sigma_0 = 34\exp(4.6E_a)(\Omega\,\text{cm})^{-1}$. The dependence of σ_0 on E_a is very weak in contrast with the laws obtained in B- and P-doped GD a-Si:H (Refs. 45–47) or even in P-doped SP a-Si:H.[7] Such laws have been interpreted by shifts of either the mobility edge or E_F with temperature.[6] Stronger effects are expected in materials containing a lower gap density of states with well-defined structures in energy in the investigated E_F range. According to this view, a weaker dependence in SP a-Si:H confirms the presence of other states than dangling bonds in the gap of SP a-Si:H and the weaker effect for B doping compared to P doping could be related to the broader valence-band tail.

The low-temperature part of the conductivity curves in highly doped samples, $Y_g = 10^{-4}$ and 10^{-3} (Fig. 10) shows a continuous curvature and it is not possible either to define an activation energy nor to fit Mott's law for variable range hopping. Our results are quite similar to those reported by Tsai[4] and interpreted by hopping con-

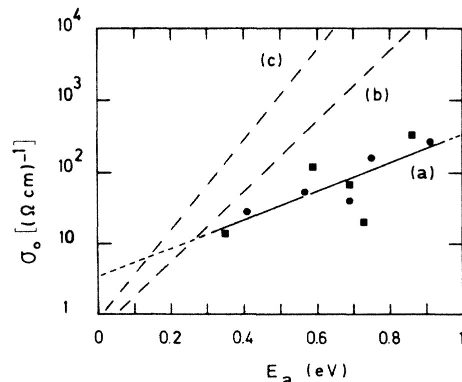

FIG. 12. Conductivity prefactor as a function of conductivity activation energy: (a) SP a-Si:H, B-doped linear fit to the data of Fig. 11; (b) SP a-Si:H, P doped, from Ref. 7; (c) GD a-Si:H, B or P doped, from various studies (Ref. 45–47).

duction through gap states occurring around the Fermi level at liquid-nitrogen temperature and gradually closer to the valence band with increasing temperature. A combination of thermoelectric power and conductivity measurements would be necessary to derive the density-of-states profile above the valence-band tail. But even thus, the derivation is not straightforward. By combining field effect and thermoelectric power measurements on B-doped GD a-Si:H, Jan *et al.*[13] were able to interpret their nonlinear conductivity curves by a double conduction path mechanism through extended states at high temperatures and through a peak of localized states at 0.42 eV above E_V at low temperature. Both interpretations do not contradict at all and equally explain our results. Further experiments using spectroscopic methods well resolved in energy would help in clarifying the existence of such a level in our sputtered samples.

Hopping conduction is obviously the dominant mechanism in the alloys ($Y_g = 10^{-2}$) in the whole temperature range. The decrease in σ_{RT} agrees with the results of Tsai[4] which show a continuous decrease with B content in the range of large-B fractions. The differences in σ_{RT} for samples deposited at 190 and 250 °C are explained by the different H contents leading to a smaller gap and higher defect density in the latter.

V. DEFECTS CHARACTERIZATION

This section is mainly devoted to the analysis of PDS and ESR results in B-doped SP a-Si:H. However, the ESR technique gives also some information on the defects in alloys that will be mentioned at the end of this section.

A. PDS

Subband-gap absorption spectra were obtained by PDS with an experimental set up described elsewhere.[48] Figure 13 shows the spectra obtained on B-doped SP a-Si:H at the different doping levels. At low doping, the results are very similar to those observed on undoped material except for a shift of the exponential edge towards higher energies. When the doping level is increased above 10^{-5}, the absorption shoulder at low energy becomes preponderant and progressively smears out the exponential part. The interpretation of the measurements involve some assumptions about the dominant optical transitions which are worth being discussed in the particular case of intrinsic or p-type materials.

The exponential part below 1.9 eV can be fitted by an Urbach law,

$$\alpha(h\nu) = \alpha_0 \exp(h\nu/E_0) . \tag{4}$$

This tail extends down to 1.5 eV in undoped a-Si:H and has been attributed to optical transitions from valence-band tail with an exponentially decreasing density of localized states toward extended states of the conduction-band.[49] The competing transitions from valence-band to conduction-band tail states bring a negligible contribution.[50] The situation remains the same for our p-type sample because the Fermi level is still far away from the valence-band and the tail states are still filled by electrons. The Urbach slope E_0 then corresponds to the characteristic energy of the valence-band tail which has been shown theoretically to depend strongly on disorder.[51]

The low-energy shoulder in undoped GD a-Si:H has been attributed to optical transitions (type I) from the singly occupied dangling-bond state T_3^0 to extended states of the conduction band.[52] But, if other kinds of gap defects are present, they will also contribute to an absorption weighted by the respective optical cross sections as recently emphasized by Bustarret *et al.*[53] The interpretation is made even more delicate in the case of boron doping. The shift of the Fermi level changes the gap state's occupation. In strongly p-type material, the deep states are empty and become the final states for electrons from the valence band (type-II transitions). At intermediate doping, both types of transitions contribute to the observed $\alpha(h\nu)$ shoulder. For these reasons, we shall not attempt any fit of $\alpha(h\nu)$ by model functions for the density of states. However, the derivation of the overall density of deep defects out of the band tails is still possible because the number of optical transitions available at a given energy depends only on the states density irrespective of their occupation. This is done by using the same procedure and calibration constant as Jackson and Amer,[52] within the first-order approximation which takes the same optical cross section of the T_3^0 state for all optically active defects.

The variations of the slope E_0 and the defect density N_R are shown in Figs. 14 and 15 as a function of the gas-

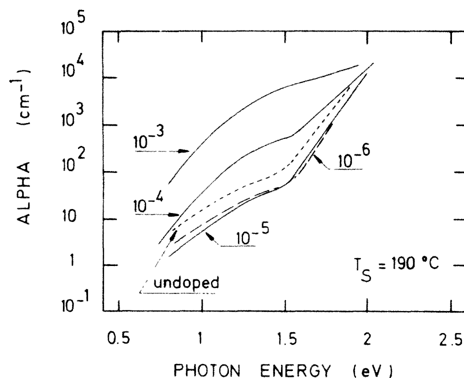

FIG. 13. Low-energy absorption spectra of B-doped SP a-Si:H deposited at 190 °C derived from PDS.

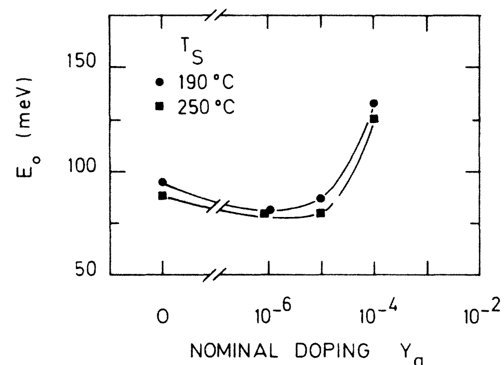

FIG. 14. Variations of the E_0 parameter as a function of gas phase dopant concentration.

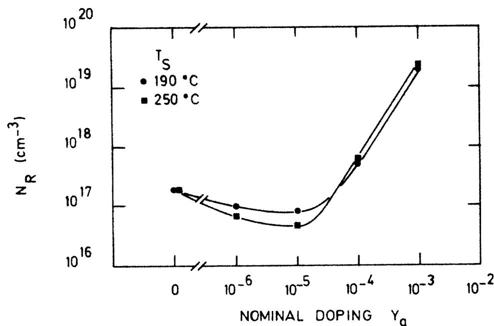

FIG. 15. Dependence of N_R on the gas phase dopant concentration.

phase dopant concentration. The minimum of E_0 obtained between 10^{-6} and 10^{-5} indicates a slight decrease of the disorder in the 1—10-ppm doping range. The N_R variations clearly show two distinct regimes: a region of decreasing defect density at low doping and another where N_R increases continuously above $Y_g \doteq 10^{-5}$. The relationship with physichemical properties and the nature of the defects will be discussed in the next section after the analysis of ESR results.

B. ESR

ESR measurements have been done at 90 K with a Varian E 12 spectrometer in the X band. The modulation frequency was 100 kHz and the field amplitude 5 G. Incident power was kept equal or below 2 mW to avoid saturation of the dangling-bond signal. Absolute determination of the spin density involved a calibration marker of P-doped monocrystalline silicon which was measured at 90 K and under the same conditions. Two traces were recorded to improve signal-over-noise ratios. During that time, temperature, klystron frequency, and magnetic field were monitored continuously to eliminate undesirable shifts of the signal. A tungsten lamp of high power equipped with an optical guide was used for light-induced experiments. The generation rate was around 10^{23} photons $cm^3 s^{-1}$.

1. Dark ESR

ESR signals are due to unpaired spins and, in the absence of illumination, vary with the density and occupation of the defects. The different signals and their variations with E_F positions have been studied extensively in GD a-Si:H by Dersch *et al.*[54] The silicon dangling-bond (DB) resonance at $g = 2.0055$ was observed only in moderate n- and p-type a-Si:H and these authors have deduced that the T_3^0 state was at or below the middle of the gap and the T_3^- state at $\sim$0.4 eV above. When E_F is shifted towards the valence band, a broad resonance appears at $g = 2.013$ which has been attributed to singly occupied states of the valence-band tail or to positively charged twofold coordinated silicon defects.[55]

The spectra of our SP-doped samples in Fig. 16 agree with this general description with slight differences in the g values: 2.0053 for the DB line and 2.009 for the broad

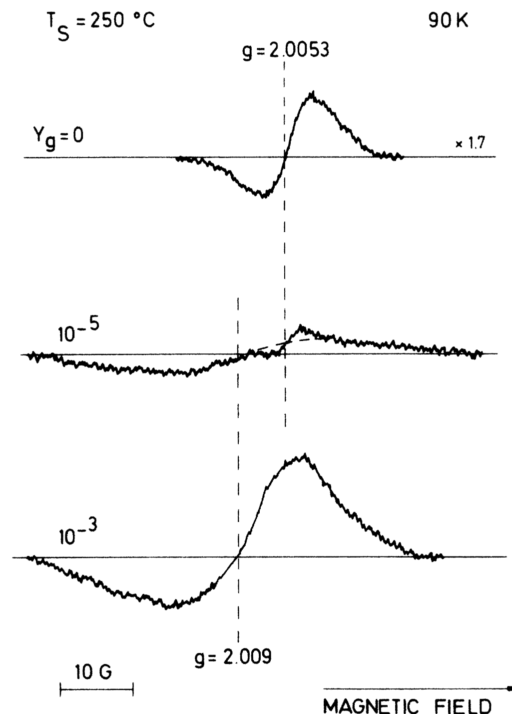

FIG. 16. ESR spectra recorded at 90 K for undoped and B-doped SP films.

line. The peak-to-peak linewidth ΔH of the broad line is between 20 and 25 G. Of course, the small signal-to-noise ratios clearly seen on the spectra when working on 1 μm thick samples give some uncertainty on g values and linewidths in the case of weak broad resonances. However, these values will be confirmed on the more intense LESR spectra. When present the narrow resonance is more easily detectable than the broad one. The curve for $Y_g = 10^{-5}$ illustrates our detection limit. The $g = 2.0053$ signal is smeared out in the noise but can still be extracted by averaging.

2. LESR

Figure 17 shows the LESR spectra for the series of sputtered films deposited at 250 °C. The results look very similar to those obtained in GD a-Si:H.[56] Generally, the signal has two components. For p-type samples, the narrow line around $g \sim 2.0053$ can be easily extracted from the broad one except for highly doped sample where a one-component signal with an asymmetrical shape is observed. The procedure could not be applied to the undoped sample because the two lines have very close g values (2.0044 and 2.0053) and ΔH (5 and 7 G, respectively). For the most intrinsic sample ($Y_g = 10^{-6}$), the narrow component is asymmetric because of the presence of these two lines in addition to the broad one. The g values, linewidths, and spin densities under the different lines estimated by assuming Gaussian line shapes are given in Table II.

The intensity of the LESR narrow line at $g \sim 2.0053$ could be used in principle as a quantitative measure of the dangling-bond density.[5] However, the determination is

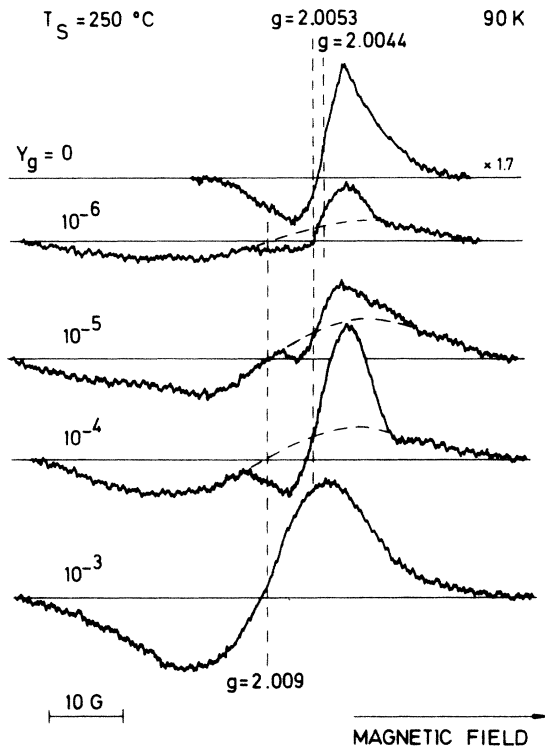

FIG. 17. LESR spectra for undoped and B-doped SP films.

subject to some limitations because it relies on the assumption that dangling bonds which were positively charged at equilibrium are converted into neutral upon the steady-state illumination. In fact, the kinetics of recombination at dangling bonds are very fast and no LESR dangling-bond signal could be observed, for example, at room temperature in agreement with recent calculations.[57] When experiments are done at 90 K, stronger signals are expected but LESR intensity measures only a fraction of the DB density especially at high densities.[5] From Figure 17 and Table II, it is clear that the concentration of DB's remains around 5×10^{16} cm^{-3} up to $Y_g=10^{-5}$ and increases significantly for $Y_g=10^{-4}$. At $Y_g=10^{-3}$, the signal is not detected because of the previous kinetics arguments.

3. *Dark ESR of a-Si-B-H alloys*

Figure 18 shows the dark ESR spectrum recorded at 90 K for a sample deposited at 250 °C and a nominal doping of 10^{-2}. It is composed of a unique broad line (23 G) centered at $g=2.0056\pm0.0004$. The spin density is 4.5×10^{18} cm^{-3}. The shape of the signal is identical at 300 K but the g value decreases to 2.0043 ± 0.0004 and the spin density to 2×10^{18} cm^{-3}. The signal from the sample deposited at 190 °C differs only by the spin density: 2.2×10^{18} and 7×10^{17} cm^{-3} at 90 and 300 K, respectively.

Similar signals have been obtained by Tsai[4] on GD samples but were not clearly attributed. We propose here to assign the signal to a boron dangling bond on the basis of the following.

(i) In a-B prepared by vapor-phase decomposition, a broad signal with $\Delta H=28$ G at 90 K and $g=2.0028$ has been measured at 90 K (Ref. 58) and the linewidth was attributed to the hyperfine interaction with the boron nuclei.

(ii) The shift of the g values from 2.0056 (SP a-Si-B-H) to 2.0028 (a-B) and intermediate values for B-rich GD a-Si-B-H can be explained by the environment of the B spin center which becomes poorer in silicon. Hydrogen atoms compensate the B dangling bonds. The DB concentration in the sample deposited at 190 °C which contains 34% H is one order of magnitude lower than in a-B.[58]

VI. DISCUSSION

We shall discuss here the results obtained in the doping regime with special emphasis on the variations of the disorder parameters and defect densities. Differences or similarities with the case of glow-discharge material will be emphasized. The particular case of alloys was discussed extensively in the previous sections and will not be reviewed.

A. Optical properties and disorder

Let us consider first the range of light doping, i.e., $Y_g\leq10^{-5}$ or $N_B\leq10^{19}$ cm^{-3}. From the evolution of the ir vibrational modes (Sec. III B 1) and variations of the optical constants (Fig. 8), we conclude that a reduction of the number of voids and a higher compactness of the Si network are achieved by the incorporation of B atoms. The increase of the optical gap (Fig. 7) in this region is mainly related to the improved local order which is achieved by the two cumulative effects of H and B. First, a better compensation of the defects is achieved by the excess amount of H provided that a sufficient mobility of the adsorbed species at the growing surface of the film allows an efficient bonding rearrangement as is the case at higher substrate temperatures. Second, according to the low doping efficiency, B atoms form essentially threefold

TABLE II. 90-K LESR spectra analysis in B-doped a-Si:H ($T_s=250$ °C).

Nominal doping	Broad line g	Broad line ΔH (G)	Broad line N_s (cm^{-3})	Narrow line g	Narrow line ΔH	Narrow line N_s (cm^{-3})	Comment
0		not seen		unresolved			2.0044 + 2.0053
10^{-6}	2.0085 ± 0.001	25 ± 5	$\sim5\times10^{17}$	2.0050 ± 0.0005	~7	6×10^{16}	asymmetrical (+ 2.0044)
10^{-5}	2.0085 ± 0.001	22 ± 5	$\sim10^{18}$	2.0050 ± 0.0005	7.5	4×10^{16}	
10^{-4}	2.0089 ± 0.0005	23 ± 5	1.1×10^{18}	2.0051 ± 0.0003	8	3.2×10^{17}	
10^{-3}	2.0092 ± 0.0003	21 ± 3	2.2×10^{18}			not seen	

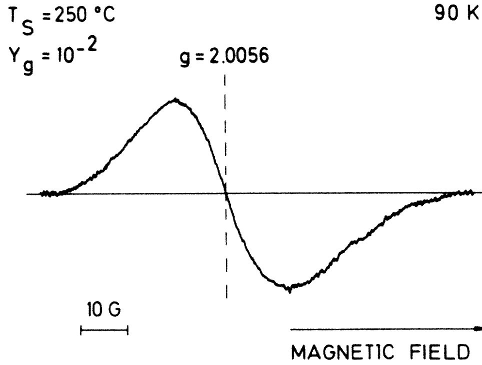

FIG. 18. ESR spectrum for an a-Si-B-H alloy sputtered at 250 °C.

coordinated covalent bonds in the Si network. Trivalent bonds are supposed to relax better the constraints of the network on a pure topological point of view.[59]

The Urbach slope E_0 is known to be the most sensitive optical parameter to short-range disorder. Figure 19(a) shows that, up to $Y_g = 10^{-5}$, E_G and E_0 are inversely correlated in agreement with the model of site disorder by Cody *et al.*[60] The linear fit to the experimental data gives $E_G = -6.2E_0 + 2.3$ eV and is parallel to the relation found by these authors from a study of isochronal annealings of GD a-Si:H. It agrees with a H- and B-related compensation of site disorder. The reduction of E_0 at low doping also fall in the correlation that had been derived for undoped SP a-Si:H between E_0 and the fraction of H in the clustered form, i.e., the r ratio defined in Sec. III B 1. This is illustrated in Fig. 19(b). Both correlations clearly indicate that the electronic properties up to the doping level of 10^{-5} are improved by the elimination of structural inhomogeneities. In particular, shallow localized states are removed from the valence-band tail (E_0 decreases) to the valence band which steepens (B_0 increases) as theoretically predicted.[51] The effect is more pronounced at 250 °C in agreement with an enhanced bonding rearrangement during growth.

The situation is very different at $Y_g = 10^{-4}$ and the previous correlations no longer hold. The compensation of

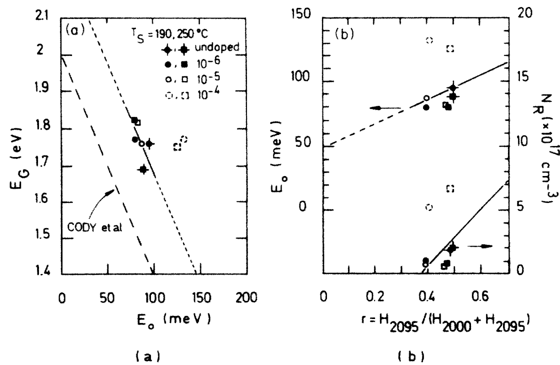

FIG. 19. Correlations of the disorder parameter E_0 and (a) the optical gap, (b) the fraction of clustered H, in the low doping range.

microvoids is still efficient and the optical gap keeps a high value but E_0 increases from 80 to 130 meV (Fig. 14). We attribute this effect to the chemical disorder brought by the B atoms with $N_B \sim 10^{20}$ cm^{-3}. This result gives a confirmation of the fact that E_0 is a better probe than E_G for detecting variations of the short-range disorder in the silicon matrix.[60] The Si-B alloying effect on the optical gap is clearly seen at $Y_g = 10^{-3}$ when [B]/[Si] ratios exceed 1%. The reason for this effect has already been explained by Tsai[4] and is summarized as follows. The Si—B bond strength of trivalent B in a matrix of tetravalent Si is lower than the Si—Si bond strength because of a covalent atomic radius 0.3 Å smaller. Thus, energy levels are expected below the Si bands.

The compensation of structural defects with doping up to $Y_g = 10^{-5}$ in SP a-Si:H was not observed in the previous studies of B doping which were done exclusively on GD materials. Although the data are very scarce, Triska *et al.*[17] have found an increase of E_0 for a 10-ppm doping and our own experiments on GD samples in this laboratory have shown that E_0 increases continuously between 60 meV for 0.3-ppm doping and 100 meV for 200-ppm doping. Moreover, an enhancement of structural inhomogeneities of the microvoids type has been inferred from studies of hydrogen effusion.[14] This behavior agrees with our correlation between E_0 and the fraction of clustered H. But in the same doping range, the optical gap still increases.[18] This can only be explained by the increase of the H content which is also observed at moderate doping in GD films. This discussion outlines the different effects of light boron doping in GD and SP a-Si:H and confirms the previous conclusion of Bruyère *et al.*[28] according to which the optical gap in SP a-Si:H is primarily determined by the H bonds rather than by the total H contents. The additional point here is the identification of clustered SiH as the main origin of the disorder.

Concerning the high doping range, there is some doubt in the literature on B doping of GD a-Si:H about the origin of the narrowing of the optical gap. The analysis of our results in Sec. IV A led us to the well-established conclusion that Si-B alloying is the main reason and that the loss of hydrogen has only a secondary effect. We believe that the same mechanism occurs in GD a-Si:H in spite of opposite opinions published recently.[18,19] The loss of H qualitatively follows the reduction of the optical gap but there is no reason why the alloying effect clearly seen in the B-rich alloys[4] could not be observed in the range of [B]/[Si] ratios of 1 at. %. Indeed, similar studies in this laboratory on the variations of E_0 and E_G for a very similar system, the GD a-Si-N-H alloys of low-N contents have shown that E_0 is already increased for a [N]/[Si] ratio of 10^{-3} while the effect of amplification of the optical gap by Si-N alloying is observed for ratios exceeding 1%.[61]

B. Electronic properties and defects

We shall now focus on the analysis of deep defects. The results of Sec. V are summarized in Fig. 20. The defect densities from PDS and ESR or LESR are plotted as a function of the solid-phase dopant concentration. We

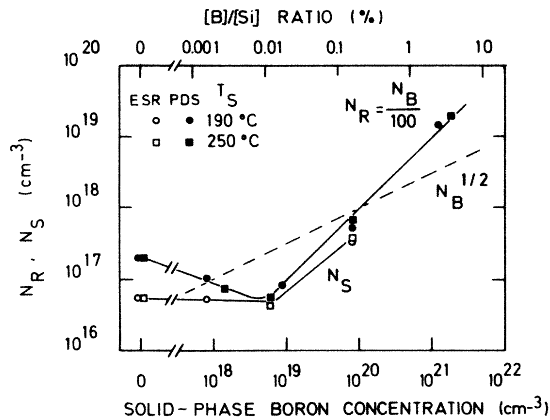

FIG. 20. Defect densities N_R and N_s as a function of solid-phase dopant concentration. N_R is measured by PDS and N_s is the maximum value between equilibrium and optically induced spin concentrations from ESR. The dashed line is for N_R in GD a-Si:H from our results and those of Ref. 5.

shall consider in turn two behaviors, as evidenced in this figure.

When the doping level increases up to $N_B \simeq 6\times10^{18}$ cm^{-3} ($Y_g=10^{-5}$) N_R decreases continuously from 2×10^{17} cm^{-3} down to 5×10^{16} cm^{-3} while N_s remains nearly constant at about 5.5×10^{16} cm^{-3}. The difference between N_R and N_s has already been attributed for undoped samples to other defects than dangling bonds associated with the presence of clustered H. This defect density N_R was shown to correlate with the ratio r defined by $r=H_{2095\,cm^{-1}}/(H_{2000\,cm^{-1}}+H_{2095\,cm^{-1}})$,[11] according to the bottom curve of Fig. 19(b). The experimental points corresponding to samples doped at $Y_g=10^{-6}$ and 10^{-5} fall roughly in this correlation especially at $T_s=190\,°C$. The compensation of microvoids upon light boron doping is so efficient that for $Y_g=10^{-5}$ and $T_s=250\,°C$, N_R compares exactly with N_s as classically found in the undoped GD materials.[52] While the relation of the extra defects to the fraction of clustered SiH is clear, the microscopic nature of the defects is still uncertain: reconstructed bonds at internal surfaces, hydrogen or impurity related defects in a void configuration are among the possibilities.

The comparison of the present results with those obtained on GD samples yields remarkable differences. Triska *et al.*[17] have noted an increase in the $\alpha(E)$ shoulder by nearly an order of magnitude for only 10 vppm B_2H_6 in SiH_4 which corresponds to $N_B\sim10^{18}$ cm^{-3} for the glow-discharge technique. The starting microscopic structure of the undoped material certainly has an effect on the onset for the regime of doping-induced defects. Our own measurements on B-doped GD films have shown that N_R was constant around 5×10^{16} cm^{-3} in the 0.3–10-vppm range and that doping induces the creation of defects only above 10 vppm. In the high doping regime, N_R increased roughly as the square root of the gas phase doping concentration as previously found by Street *et al.*[5] (dashed line of Fig. 20). In GD a-Si:H, the square-root dependence on gas phase dopant concentration has been also verified for P (Refs. 5 and 49) and As doping,[62] and so appears to be a general feature of doping process in this material. Instead of that, we obtain in the SP material a linear dependence in the form $N_R=N_B/100$. It is not really surprising to find a different law for GD and SP a-Si:H. The interpretation of the square-root law given by Street[63] is based on a thermal-equilibrium argument for the interaction of dopants with dangling bonds at the growing surface. This could hardly apply to the sputtering deposition which is a process much further from equilibrium. In particular, ionic bombardment must play an essential role in the incorporation mechanism of the dopants. This would explain why the dopant incorporation is linear and does not depend on the substrate temperature. Now, the linear dependence of N_R versus N_B could be explained in the simplest way if statistically one B atom over a hundred is incorporated in a configuration where it creates an extra defect. Experiments on compensated samples would be very helpful to know if the Fermi-level position itself plays a role in the defect creation mechanism as it is obviously the case for GD a-Si:H.

The comparison between the absolute N_R densities for SP and GD materials (Fig. 20) shows that in a certain doping range SP a-Si:H has a lower gap defect density than GD a-Si:H. In particular, at $N_B\sim10^{19}$ cm^{-3} this advantage reaches nearly an order of magnitude. This result has a technological interest because it demonstrates that highly resistive materials (Fig. 9) with low defect densities can be obtained by sputtering amorphous silicon in a mixture containing a few vppm's of diborane.

From the increase of the LESR spin density at $Y_g=10^{-4}$ and $N_s\simeq N_R$ (Fig. 20), we can say that the doping-induced defects are dangling bonds. The same conclusion was found for GD a-Si:H from the different studies on B doping. However, Jan *et al.*[13] have concluded that the density of localized states lying 0.42 eV above the valence band increases for $[B_2H_6]/[SiH_4]$ ratios exceeding 10^{-4} and ascribed it to B acceptors. In the light of our results, we should like to suggest two possible explanations for these observations. A nominal doping of 10^{-4} for GD a-Si:H leads to $N_B\simeq2\times10^{19}$ cm^{-3}. A similar B content would be obtained in our SP films at $Y_g=4\times10^{-5}$ (Fig. 1) which is around the doping level where the transition from a single-channel transport to a two-channel transport behavior occurs (Fig. 10). The broadening of the valence-band tail and the increase in the DB density also occur around this level. The first possibility is that the states observed by Jan *et al.*[13] are the Si—B bonding states associated with the threefold coordinated B atoms. Their position in energy between 0.3 and 0.45 eV above E_v (Ref. 13) agrees with the shrinking of the optical gap by nearly 0.3 eV that is observed at $N_B\simeq10^{21}$ cm^{-3} either in SP (Fig. 7) or GD (Ref. 18) materials when the local density of Si-B states is sufficiently high to shift the valence-band edge. The second possibility involves only dangling bonds. We suggest that the dangling bonds induced by doping have different energy levels from those in pure a-Si:H. This could arise from the defect creation mechanism itself. The reaction $B_3^0+T_4^0\rightarrow T_3^+$ is not only favorable according to the modified 8-N rule[63] but also induces a lowering of the dangling-bond energy by Coulomb attraction if the ion-

ized atoms are neighboring. Indeed, some deep level transient spectroscopy (DLTS) experiments by Cullen *et al.*[64] on P-doped GD a-Si:H counterdoped by B have shown that a peak in the density of states at 1 eV below E_c was progressively reduced with increasing B doping while a new structure at 1.4 eV below E_c was developed. This last energy position agrees with that of Jan *et a.*[13] Such levels were hardly resolved by DLTS and the broad shoulder in the $\alpha(h\nu)$ PDS spectra cannot be used to precisely deduce structures in the gap density of states as discussed in Sec. V A. Space-charge spectroscopies on p-type samples are very delicate but would still be the most reliable techniques to test our suggestions, and further work is needed in that direction.

VII. SUMMARY AND CONCLUSIONS

Amorphous silicon films sputtered in a wide range of $[B_2H_6]/(Ar+[H_2])$ concentrations have been characterized through a great variety of techniques resulting in the simultaneous knowledge of chemical composition, H bondings, optical and electrical properties, gap defect density, and valence-band characteristic energy. The results lead us to distinguish three regimes according to the boron concentration.

(i) A low doping regime: $Y_g \leq 10^{-5}$, $N_B \leq 6\times 10^{18}$ cm^{-3}. Two gettering effects are observed: first, diborane at 1-vppm concentration in the plasma is responsible for a marked increase in the H content; second, the hydrogen is preferably incorporated as diluted Si—H and SiH_2 units and the fraction of H in the clustered form is considerably reduced with respect to that of the undoped samples. The slight increase of the optical gap is primarily determined by the latter effect and is accompanied by a decrease of the E_0 parameter. The correlations between E_0 or N_R from PDS and the fraction of clustered H from ir spectroscopy previously found in undoped material still apply at moderate doping. In this range, the concentration of dangling bonds measured by ESR remains at a constant level. For $N_B \sim 10^{19}$ cm^{-3}, the defect densities measured either by PDS or ESR are well below the values measured on GD a-Si:H with the same B content.

(ii) A heavy doping regime: $10^{-5} < Y_g \leq 10^{-3}$, $10^{19} \leq N_B \leq 2\times 10^{21}$ cm^{-3}. The chemical disorder is responsible for a broadening of the valence-band tail for [B]/[Si] ratios exceeding 0.1 at. %. The optical gap narrowing observed for a ratio of 1 at. % is explained by Si-B alloying rather than the loss of hydrogen that we have followed by the nuclear reaction. The low doping efficiency implies that B atoms are essentially threefold coordinated in the tetravalent Si network. Thus, energy levels below the Si bands are introduced. The conductivity still increases through significant shifts of the Fermi level and reaches values comparable to those obtained on GD a-Si:H. At and below room temperature, the contribution of transport via localized states predominates and suggests a broadening of the valence-band tail or an increase of deep defects density. PDS measurements show that both effects actually occur because of the chemical disorder and of the emergence of new defects, respectively. A linear relationship $N_R = N_B/100$ is found between the defect density and the solid-phase boron concentration. Instead of the mechanism proposed by Street,[63] we propose that ionic bombardment plays the essential role in the incorporation of dopants by the sputtering technique as the same linear incorporations of B into the films and the same defect densities were measured for the two series of samples deposited at 190 and 250 °C. LESR experiments identify the new defects as being mainly dangling bonds. A shift of the dangling-bond energy in this configuration has been proposed to account for the existence of energy levels at $\sim$0.4 eV above E_v in B-doped GD materials.[13,64]

(iii) An alloy regime: The transition between doping and alloying occurs for [B]/[Si] ratios higher than 5%. The a-Si-B-H alloys have a higher total hydrogen content and exhibit ir spectra totally different from those of B-doped a-Si:H. The different lines have been identified and the existence of a high fraction of polyhydride units explains the low density of the material. The connectivity of the network is partly realized through bridging B—H—B or Si—H · · · B bonds. ESR active defects in high density were identified as boron dangling bonds in various environments. These materials are much more resistive than B-doped a-Si:H. Their optical gap seems to depend strongly on the hydrogen content as is the case for a-B:H.

ACKNOWLEDGMENTS

We wish to thank F. Lesimple from Thomson-C.S.F.—St. Egrève for SIMS measurements and A. Dias (University of Lisboa) for the thermoelectric power measurements. P. Siffert (Centre de Recherche Nucléaire, Strasbourg), J. Magarino (Thomson-C.S.F.—Corbeville), and A. Hervé (Centre d'Etudes Nucléaires, Grenoble) are gratefully acknowledged for kindly providing the facilities of nuclear reaction, PDS and ESR, respectively. Thanks are due to C. Bianchin, H. Matraire, R. Biraghi, and E. Boissonnet for their technical assistance, and to J. C. Bruyère and F. Boulitrop for helpful discussions and critical reading of the manuscript.

[1]W. E. Spear and P. G. LeComber, Solid State Commun. 17, 1193 (1975).
[2]W. Paul, A. J. Lewis, G. A. N. Connell, and T. D. Moustakas, Solid State Commun. 20, 969 (1976).
[3]W. E. Spear and P. G. LeComber, Philos. Mag. 33, 935 (1976).
[4]C. C. Tsai, Phys. Rev. B 19, 2041 (1979).
[5]R. A. Street, D. K. Biegelsen, and J. C. Knights, Phys. Rev. B 24, 969 (1981).
[6]W. Beyer and H. Overhof, in *Semiconductors and Semimetals*, edited by J. I. Pankove (Academic, New York, 1984), Vol. 21, Pt. C, p. 257.
[7]D. A. Anderson and W. Paul, Philos. Mag. B 45, 1 (1982).

[8]M. J. Thompson, J. Allison, M. M. Alkaisi, and I. P. Thomas, Rev. Phys. Appl. **13**, 625 (1978).
[9]P. Viktorovitch, D. Jousse, A. Chenevas-Paule, and L. Vieux-Rochas, Rev. Phys. Appl. **14**, 201 (1979).
[10]T. D. Moustakas and R. Friedman, Appl. Phys. Lett. **40**, 515 (1982).
[11]D. Jousse, E. Bustarret, and F. Boulitrop, Solid State Commun. **55**, 435 (1985).
[12]D. Jousse, Ph.D thesis, Université Scientifique, Technologique et Medicale de Grenoble, 1986 (unpublished).
[13]Z. S. Jan, R. Bube, and J. C. Knights, J. Appl. Phys. **51**, 3278 (1980).
[14]W. Beyer, H. Wagner, and H. Mell, Solid State Commun. **39**, 375 (1981).
[15]F. J. Demond, G. Muller, H. Damjantschitsch, H. Mannsperger, S. Kalbitzer, P. G. LeComber, and W. E. Spear, J. Phys. (Paris) Colloq. **42**, C4-779 (1981).
[16]S. G. Greenbaum, W. E. Carlos, and P. C. Taylor, Solid State Commun. **43**, 663 (1982); J. Appl. Phys. **56**, 1874 (1984).
[17]A. Triska, I. Shimizu, J. Kocka, L. Tichy, and M. Vanecek, J. Non-Cryst. Solids **59/60**, 493 (1983).
[18]I. Wagner, H. Stasiewski, B. Abeles, and W. A. Lanford, Phys. Rev. B **28**, 7080 (1983).
[19]J. Ristein and G. Weiser, Sol. Energy Mater. **12**, 221 (1985).
[20]H. Hamdi, A. Deneuville, and J. C. Bruyère, J. Phys. (Paris) Lett. **41**, L-483 (1980).
[21]D. Jousse, J. Said, and J. P. Stoquert, Thin Solid Films **124**, 191 (1985).
[22]M. Toulemonde, P. Siffert, A. Deneuville, and J. C. Bruyère, Appl. Phys. Lett. **39**, 152 (1981).
[23]M. H. Brodsky, M. Cardona, and J. J. Cuomo, Phys. Rev. B **16**, 3556 (1977).
[24]E. C. Freeman and W. Paul, Phys. Rev. B **20**, 716 (1979).
[25]G. Lucovsky, R. J. Nemanich, and J. C. Knights, Phys. Rev. B **19**, 2064 (1979).
[26]H. Shanks, C. J. Fang, L. Ley, M. Cardona, J. F. Demond, and S. Kalbitzer, Phys. Status Solidi B **100**, 43 (1980).
[27]H. Wagner and W. Beyer, Solid State Commun. **48**, 585 (1983).
[28]J. C. Bruyère, A. Deneuville, A. Mini, J. Fontenille, and R. Danielou, J. Appl. Phys. **51**, 2199 (1980).
[29]G. Lucovsky, Sol. Cells **2**, 431 (1980).
[30]S. C. Shen and M. Cardona, Phys. Rev. B **23**, 5322 (1981).
[31]W. C. Price, J. Chem. Phys. **16**, 894 (1948).
[32]I. Freund and R. Halford, J. Chem. Phys. **43**, 2795 (1965).
[33]N. A. Blum, C. Feldman, and F. G. Satkiewicz, Phys. Status Solidi A **41**, 481 (1977).
[34]A. A. Berezin, O. A. Golikova, M. M. Kazanin, T. Khomidov, D. N. Mirlin, A. V. Petrov, A. S. Umarov, and V. K. Zaitsev, J. Non-Cryst. Solids **16**, 237 (1974).
[35]J. I. Pankove, P. J. Zanzucchi, C. W. Magee, and G. Lucovsky, Appl. Phys. Lett. **46**, 421 (1985).
[36]N. W. Johnson, Phys. Rev. B **31**, 5525 (1985).
[37]W. Richter, W. Weber, and K. Ploog, J. Less-Common. Metals **47**, 85 (1976).
[38]W. Paul and D. A. Anderson, Sol. Energy Mater. **5**, 229 (1981).
[39]N. Morita and A. Yamamoto, Jpn. J. Appl. Phys. **14**, 825 (1975).
[40]F. H. Cocks, P. L. Jones, and L. Dimmey, Appl. Phys. Lett. **36**, 970 (1980).
[41]I. Solomon, T. Dietl, and D. Kaplan, J. Phys. (Paris) **39**, 1241 (1978).
[42]T. D. Moustakas, Proceedings of the Fifth EC Photovoltaic Conference, Athens, Greece, 1983 (unpublished).
[43]G. H. Bauer and G. Bilger, *Proceedings of the Fourth EC Photovoltaic Solar Energy Conference,* edited by W. H. Bloss and G. Grassi (Reidel, Dordrecht, 1982), p. 773.
[44]N. V. Dong and T. Q. Hai, Phys. Status Solidi B **88**, 555 (1978).
[45]D. E. Carlson and C. R. Wronski, in *Amorphous Semiconductors,* Vol. 36 of *Topics in Applied Physics,* edited by M. H. Brodsky (Springer, New York, 1979), p. 287.
[46]D. I. Jones, P. G. LeComber, and W. E. Spear, Philos. Mag. B **35**, 1173 (1977).
[47]H. Fritzsche, Sol. Energy Mater. **3**, 447 (1980).
[48]F. Boulitrop, J. Bullot, M. Gauthier, M. P. Schmidt, and Y. Catherine, Solid State Commun. **54**, 107 (1985).
[49]C. R. Wronski, B. Abeles, T. Tiedje, and G. D. Cody, Solid State Commun. **44**, 1423 (1982).
[50]D. Redfield, Solid State Commun. **44**, 1347 (1982).
[51]J. Singh, Phys. Rev. B **23**, 4256 (1981).
[52]W. B. Jackson and N. M. Amer, Phys. Rev. B **25**, 5559 (1982).
[53]E. Bustarret, D. Jousse, C. Chaussat, and F. Boulitrop, J. Non-Cryst. Solids **77/78**, 295 (1985).
[54]H. Dersch, J. Stuke, and J. Beichler, Phys. Status Solidi B **105**, 265 (1981).
[55]For a review, see P. C. Taylor, in *Semiconductors and Semimetals,* edited by J. I. Pankove (Academic, New York, 1984), Vol. 21, Pt. C, p. 136.
[56]R. A. Street and D. K. Biegelsen, J. Non-Cryst. Solids **35/36**, 651 (1980).
[57]F. Vaillant and D. Jousse, Phys. Rev. B **34**, 4088 (1986).
[58]G. Gewinner, L. Kubler, J. J. Koulmann, and A. Jaegle, Phys. Status Solidi B **70**, 595 (1975).
[59]J. C. Phillips, Phys. Rev. Lett. **42**, 1151 (1979).
[60]G. D. Cody, T. Tiedje, B. Abeles, B. Brooks, and Y. Goldstein, Phys. Rev. Lett. **47**, 1480 (1981).
[61]E. Bustarret (unpublished).
[62]R. A. Street, J. Non-Cryst. Solids **77/78**, 1 (1985).
[63]R. A. Street, Phys. Rev. Lett. **49**, 1187 (1982).
[64]P. Cullen, J. P. Harbison, D. V. Lang, and D. Adler, J. Non-Cryst. Solids **59/60**, 261 (1983).